Al-Furat Journal of Innovations in Electronics and Computer Engineering (FJIECE)
ISSN -2708-3985

Classification of Melanoma Based on Clustering Channels RGB of Skin Scan Using Adaptive Light Weight Deep Learning System

Ammar Wisam Altaher

Department of Information Technology, Management Technical College, Al-Furat Al-Awsat Technical University, Iraq
Dr.ammar@atu.edu.iq

https://doi.org/10.46649/fjiece.v3.1.8a.17.4.2024

Abstract. *Melanoma is considered to be a type of skin cancer that is characterised by symptoms of poor prognostic responses. In this paper, we propose a deep learning method using DCNNs, modifying the output layer and enhancing the features of skin scan images collected from Kaggle to be distinguished into two groups: melanoma and non-melanoma cells. The proposed modified three types of DCNN (MobilNet-v2, ResNet-18 and Squeeze Net) models have been tested in two experiments. In the first, the obtained values of training accuracy are (93, 95 and 91) % and the testing accuracy is (90.09, 90.54 and 90.4) %, using original datasets only. In the second experiment, the obtained values of training accuracy are (99.7, 96.3 and 92) % and the testing accuracy is (94.41, 94.14 and 91.43) %, The experimental findings show that the model utilized produces enhanced photos with more accuracy than original images.*

Keywords: *Deep Learning (DL), Light Weight Convolutional Neural Networks (LWCNN), Melanoma Classification*

1. INTRODUCTION

Skin cancer has been a diffused disease worldwide. In recent decades, the appearance of melanoma or non-melanoma skin cancers has increased [1]. According to some references, the reduction of skin cancer happens when the growth of skin cells is out of control. Not Melanoma skin cancers are usually clustered as non-melanoma skin cancers [2]. The type of cancer that starts with pigment cells of the skin is called melanoma. Pigmented moles or marks that appear on the skin represent melanoma. It could be extended to other organs of the body. The main cause of melanoma is excessive exposure to the sun [3]. Over the last few years, convolutional neural networks (CNNs) have become precious tools for the classification of biomedical images and clinical diagnosis in multiple fields such as ophthalmology, histology, dermatology and radiology. Widespread deep learning techniques, especially CNNs, make the process of diagnosing these complex diseases easier, without the need for experts to deal with them or to understand their principles [4]. From a mathematical point of view, weights are millions of configurable parameters of functions called deep neural networks. For a task of image classification, these weights are changed where the pixel intensities of an input image are assigned to a class label probability [5].

In medical imaging, CNNs are the most popularly adopted algorithms and are used for multiple tasks such as the classification of images, detection of objects, and super-resolution. However, the bulk of accurate computer-aided diagnoses is image segmentation [6], To gain a segmentation mask and CNN network, a Classical K-means classifier is used; a CAD system is also used in the detection of melanoma. The necessity of keeping the region of interest (ROI) to make Classification performance, depends on detecting the skin lesion and cutting Remove any unnecessary areas from the image. The aim of detecting a single melanoma and classifying it is different from the detection of objects with multi-class in a large image, which provides a high ratio of the area in the clinical image [7].

Our participation includes First, we provide a fully automated feature extraction-based melanoma detection approach. Next, following classification using ResNet 18 and thorough evaluation, carry out a thorough assessment of our model's efficacy and generalization capacity using HAM10K. Second, in order to achieve a high degree of classification accuracy, our suggested approach focuses on segmenting and improving medical images. In the end, we have developed a novel approach for training large datasets on low-end computing resources.

2. RELATED WORK

The concept of using Convolutional Neural Networks, used an approach in case-based reasoning (CBR) system for the classification of skin lesions and early detection of melanoma. DePicT melanoma Deep-CLASS is a proposed system where the input images are retrieved to provide users with recommendations associated with their desired problem such as images of the affected area. The main component of DePicT Melanoma Deep-CLASS is CNN with sixteen layers and two additional layers; one for input and the other for output, which could be learned and trained. Three main characteristics in DePicT melanoma Deep-CLASS assist and enhance this system, Equivariant representations, and Sparse interactions. Within the framework of using deep neural networks, a classification of skin lesions using a single CNN is demonstrated in [8], Two cases are used in this approach: the first represents common cancer correspondence; and the second represents the deadliest skin cancer correspondence. In [9], transfer learning for classification is used. The principle of transfer learning is to begin from patterns that have been learned previously from variant problems rather than beginning from scratch. Transfer learning is usually performed with the use of models that are pre-trained in the classification of images. The pre-trained weights which are used as pre-trained models are Inception ResNet v2, ResNet 152, and Inception v3. In this system, Inception ResNet v2 architecture is used as a pre-trained model to achieve the best results on all layers and replace one fully connected, one global average pooling, and a softmax layer with top layers that allow classifying only two categories. Depth-wise Separable Convolution, which is a separable depth-wise filter, represents the main part of MobileNet.

Pre-processing of the image dataset is used in [10]. RGB plane masking operation and thresholding segmentation are the main considerations of this system. By using threshold segmentation, the image is converted into a binary image. Some of the features are extracted, namely, shape, entropy and energy. Classification using Inception V3 CNN and Inception V4 CNN is used [11]. In this approach, the extracted features from CNN are combined with other features like colour and texture, which are obtained from the lesion region of the images. Class probabilities and two bounding boxes are generated in YOLO and a single CNN can make multiple bounding boxes and class probabilities for the Region of Interest (ROI). Full images are used in YOLO-CNN to optimise the detection performance. YOLO is characterised by three characteristics: its speed. The optimisation process in this architecture is performed with RMSprop, by considering the merit of parallel computing on GPUs. In the training phase, melNET adopts the backpropagation method with the Inception-v3 model by feeding the errors from each iteration, reaching to fine-tuning weights of the network. The prediction or diagnosis of the model is executed by inputting lesion images into the system. Main goal of architecture is enhance performance by increasing the dimensions of the network without any sudden load on computation. An automatic skin lesions classification method is presented [12].

In this approach, AlexNet is used in various ways with the transfer learning consisting of fine-tuning weights of model, GoogLeNet is modified and presented in where the data is sent for the inception block from the previews layer. As a result, at the end of these parallel operations, each output is combined as input for the next layers of this CNN. To overcome the overfitting problem, this architecture uses inception modules instead of fully connected layers. A combination of CNN with ANN is proposed in [13], this framework consists of pre-processing data as a first stage. To get the best decision, two different classification algorithms are combined CNN and ANN. There is a very small percentage of the view for

dermatologic lesions, therefore, the lesions could be too tiny to be recognised if the scale of the image is decreased. The next step is the use of bilinear interpolation to recognise images into 300×300 pixels. The last step in this architecture is the admiration of CNN on the increase of fly data such as vertical and horizontal flips, zoom (90–110% of length and width) and random rotation (-10, +10) to boost the dataset. To increase the performance of classification, authors in [14] used both spatial and spectral. Two identical hyperspectral imagers are used to collect hyperspectral images. The separation of Spectral from images is according to the Fabry-Perot Interferometer (FPI). The advantage of using FPI is that it helps in making fast spectral domain scanning. The wavebands of the imager are from 450 nm to 850 nm. The problem statement is related to the classification of skin images into melanoma and non-melanoma classes using deep learning techniques. The research aims to develop a robust and accurate model that can effectively differentiate between these two classes based on skin scan images. The study focuses on enhancing the features of the images to improve the classification performance and ultimately contribute to the early detection of melanoma, a type of skin cancer.

3.DATASET AND METHODS

In this paper, four stages are adopted as part of the methodology: obtaining the dataset, preprocessing data, feature extraction, and classification. where the implemented framework for CNN-based skin image classifiers is performed using machine specifications, 8 GB DDR4 RAM, and CPU Ryzen 5 using MATLAB 2021a. 3550H, GFX 2.10 GPU with Windows 10.

3.1 Dataset

The skin images dataset was acquired from Kaggle, it is a dataset including two classes (melanoma and non-melanoma), and each class has the same number of images. In the source dataset, classes are divided into three folders (train, test, valid) because the dataset was trained using Python. In this study, we combined all these folders into one folder using MATLAB as in Table 1.

Table 1. Characteristics of the Dataset.

Types	Train	Test	Valid	Sum
Melanoma	5341	1781	1781	8903
Nonmelanoma	5341	1781	1781	8903

In the dataset, 80% of images are used to train the model and 20% are used for validation. The training process is performed on three levels to reduce the number of used resources.

3.2 DCNNs

3.2.1 MobilNet-v2

MobileNetV2 has 53 layers deep, as illustrated in Fig. 2, and requires 3.5 million operations with a parameter size of 13 MB [15–16]. It is an advancement over the previous MobileNet and MobileNetV1 versions, which were meant for embedded use. A small accuracy loss results from the simplicity, which is looked into. Both architectures can categorize photos into up to 1000 item types because ImageNet has assessed their performance.

Al-Furat Journal of Innovations in Electronics and Computer Engineering (FJIECE)
ISSN -2708-3985

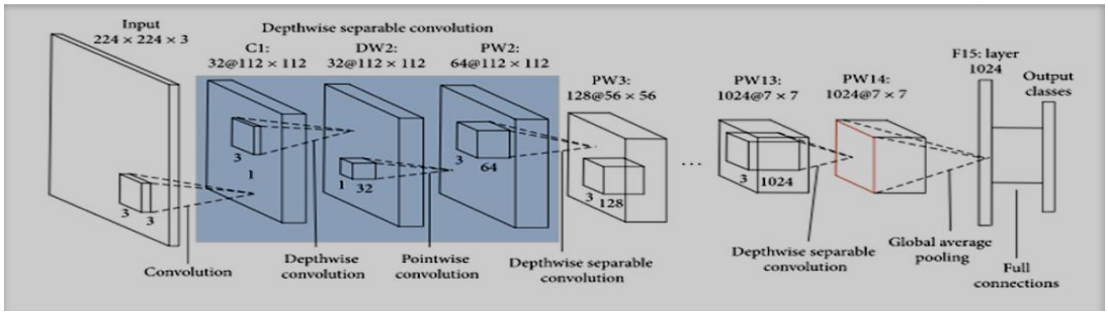

Figure 1: ResNet-18 Structure [17].

3.2.2 ResNet-18 Model

ResNet-18 is a type of deep neural network that uses skip connections or shortcuts that pass through some layers. In ResNet-18, a residual block is the main structure consists of 71 layers and 78 connections in 8 residual building blocks, as shown in Fig 2. [17].

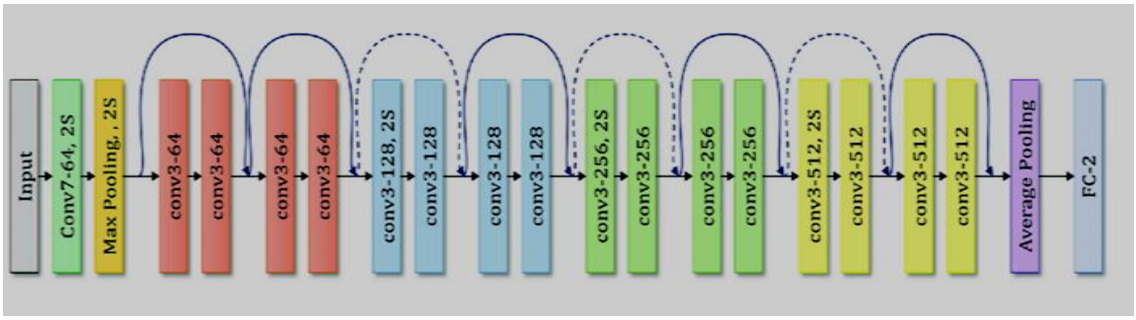

Figure 2: ResNet-18 Structure.

A type of shortcut is utilised to skip the convolutional layer [18]. Output and input vectors through the convolutional layer can be directly added [19]. A ResNet-18 model was introduced in 2015 [20]. Moreover, it has structures like the brain's cerebral cortex [21].

3.2.3 SqueezeNet

As we only have two classes, despite having 50 times fewer parameters than AlexNet, it has an excellent accuracy . As seen in Fig 3, SqueezeNet has 18 layers and can categorize photos into up to 1,000 different item categories.

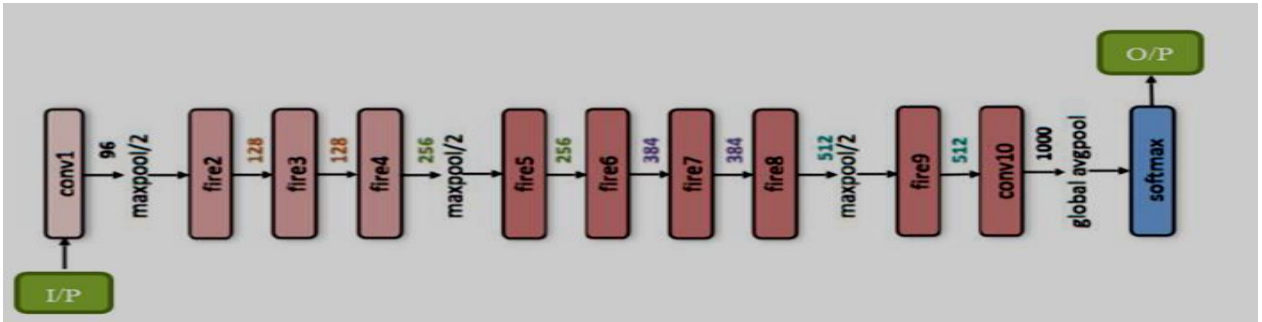

Figure 3: SqueezeNet CNN Architecture.

Al-Furat Journal of Innovations in Electronics and Computer Engineering (FJIECE)
ISSN -2708-3985

Fig 3 shows the SqueezeNet architecture. It starts with a solo convolution layer (conv1), A Fire module consists of an enlarged layer with a combination of 1x1 and 3x3 convolution filters feeding into a squeeze convolution layer.

3.3 Analysis of Skin Scan Images

We provide sufficient number databases to overcome the disadvantages of extracting features and obtaining high resolution. To achieve our aim, we used two experiments: Frist experiment, realisation for all datasets is executed from the original size, to be performed using the CNN proposed model. Next, we divided each dataset class in half, using 80% for training and 20% for testing. As seen in Fig 4. The training dataset is then supplied to ResNet-18 for training.

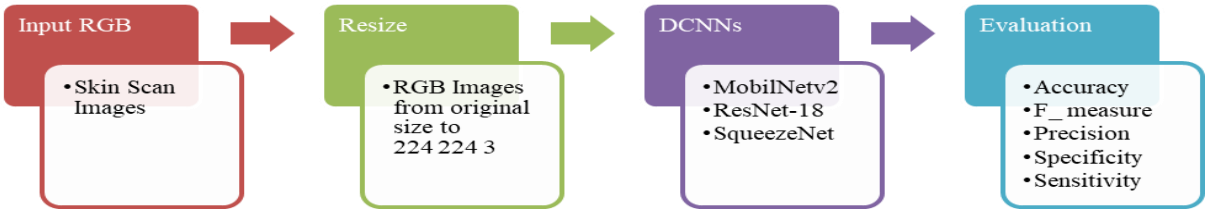

Figure 4: Flow diagram of the Proposed Method to Train the Original Dataset on ResNet-18 to Experiment (1).

second experiment used the same split class of dataset as the first experiment (80% for training and 20% for testing). We added some utilised image enhancement techniques to enhance the quality of the input images. The methods include morphological structuring [22-24], clustering channels RGB, LAB-image, RGB image, and histogram equalization [25], The final step before training the new dataset, rotating all images 5 degrees to obtain data augmentation.

Now, We will explain all the techniques used:

3.3.1. Morphological structuring

Image segmentation is done using morphological processes. Finding areas in a picture that represent things or significant portions of objects is known as image segmentation. The filling of minor gaps in objects, the division of almost overlapping or neighbouring items, and the reunification of broken borders into continuous segments are typical uses for morphological operators. The formula used to decide whether to operate the pixels using erosion or dilation [26]

3.3.1.1. Dilation:

The value of the output is equal to the sum of all the values of the nearby pixels to the input pixel. As shown in Fig.5, in a binary picture, if any pixel is assigned to the value 1, the output pixel is also set to 1.

Al-Furat Journal of Innovations in Electronics and Computer Engineering (FJIECE)
ISSN -2708-3985

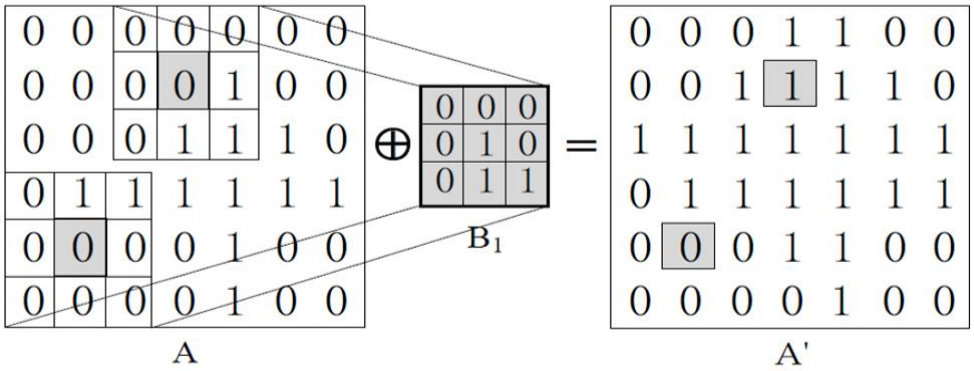

Figure 5: Morphological Dilation Operator Binary Image A by Structuring Elements B1.

3.3.1.2. Erosion:

The total of all the values of the pixels that are close to the input pixel determines the value of the output pixel. In a binary image, as shown in Fig. 6, if any of the pixels are set to 0, the output pixel is likewise set to 0.

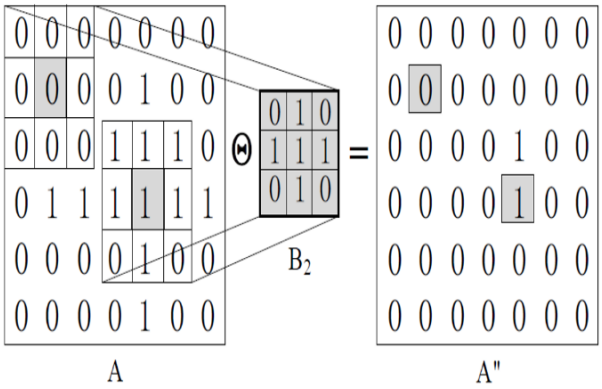

Figure 6: Morphological Erosion Operator of Binary Image A by Structuring Elements B2.

In our study, we used the erosion type of morphological operation with a 7*7 structuring element in the type of desk. Moreover, Generally, structural elements that are two-dimensional or flat are significantly smaller than the image that is being processed. A tool for segmentation is MATLAB, which is software designed for high-performance languages in technical computing [27]. A morphological structuring element is created using the MATLAB function "Strel," as seen in Equation 1 and Figure 7. The syntax for the structural element, SE, is as follows:

SE = strel (Desk,7) *(1)*

Al-Furat Journal of Innovations in Electronics and Computer Engineering (FJIECE)
ISSN -2708-3985

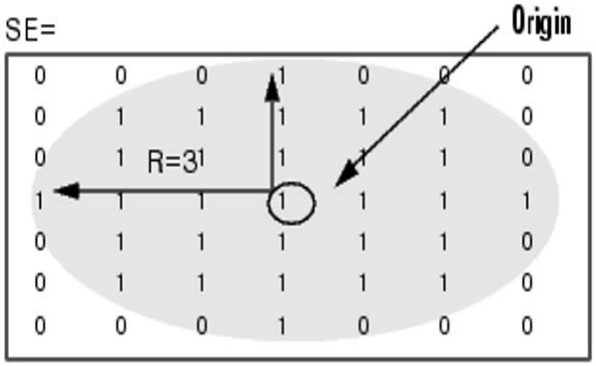

Figure 7: Disk Structuring Element.

Where parameters are a list of characteristics that describe the shape's size information and shape is a string indicating the desired shape. The supported forms are all included in this table. The characteristics that strel can take vary depending on the form. The details of how to make each type of structural element follow [28].

3.3.2. Clustering Color

This process is similar to k-means clustering which is used to classify a set of things based on certain features or characteristics. Thus, we can classify the image channels based on their basic components (RGB), as shown in Fig 8. Then will convert it into a binary image. Each channel in the image has become an independent image with two dimensions but it carries one single color. This operation removes all noise on the skin scan images such as hair. It then, combined RGB channels to produce new colour images after cleaning each channel from noise. In this way, we have produced a new dataset that has clear advantages for computers that enable them to easily identify them and train the simple network and get higher results compared to other methods or when using real data taken directly from the skin.

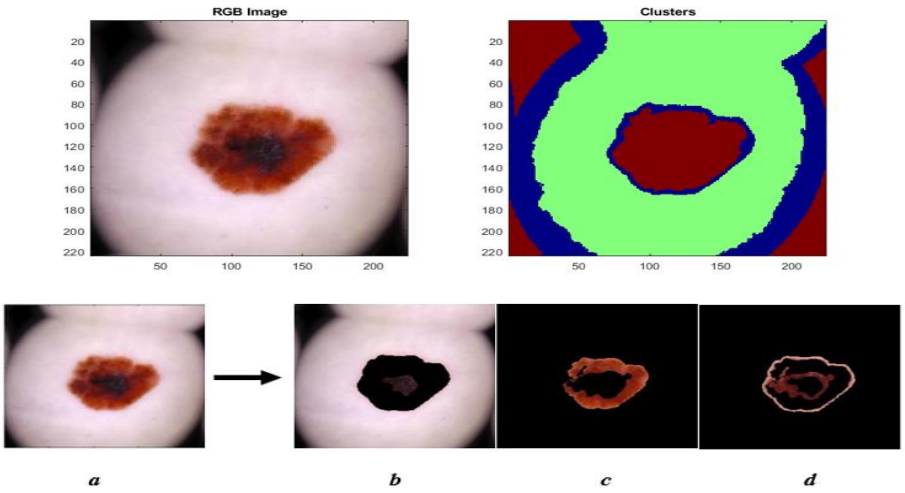

Figure 8: The process of Separating the Image Channels into RGB. (a. original image, b. R-channel, c. G-channel and d. B-channel).

3.3.3. Unsharp filter

The unsharp filter is a fundamental sharpening operator that improves an image's edges and other high-frequency elements by deducting a smoothed-out or unsharp copy of the original picture. The unsharp filtering process is widely employed in the photographic and printing industries to sharpen the corners. Using the following Eq (2), un sharp masking creates an image g (x,y) from an input image fx.

$$g(x,y)=f(x,)-f\ smooth(x,y) \qquad (2)$$

3.3.4. Histogram Equalization

This method is the second phase in the study's process for enhancing contrast by altering the intensities of skin scan pictures. When a picture represented by an intensity value range that limited, this method often boosts the overall contrast of multiple images. The method, can improve the effectiveness of structure in skin scan photos as well as the detail in either overexposed or underexposed shots, as shown below in Fig 9. the intensities The histogram can be more consistently distributed, using the entire range of intensities. This allows locations with low local contrast to acquire higher contrast.

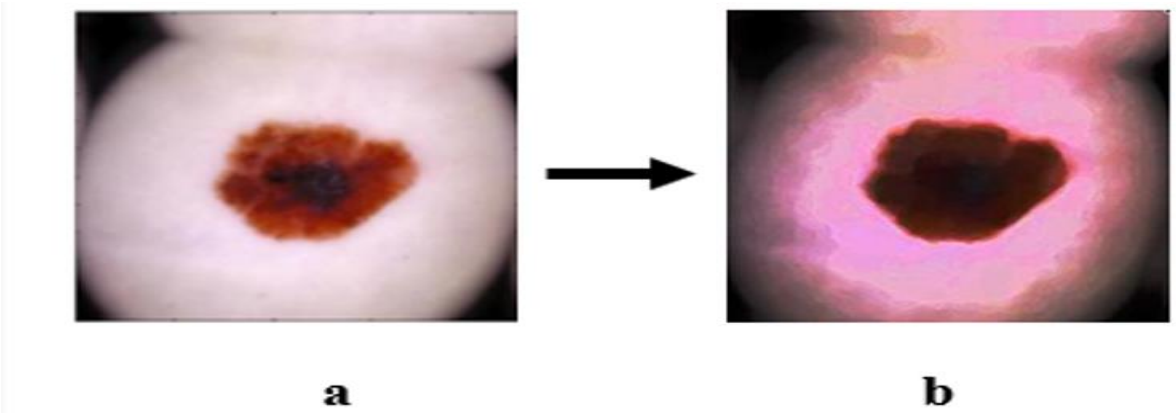

Figure 9: The process of Producing a New Colour Image After Applying the Unsharp Filter and Histogram Equalization (a.oraganal image, b. new image).

3.4 Transfer Learning

Transfer learning is used in the proposed classifier's CNN model to increase learning effectiveness [29-31]. Transfer learning is the process of transferring and reusing knowledge acquired while resolving one problem to address another. We must develop two elements to carry out transfer learning:

- The network architecture is shown as a series of layers. This is made by making changes to an already-existing network, such as ResNet-18.
- A dataset of skin photos with specified labels will be utilized as training data, which is often made available through data storage.

4.EXPERIMENTAL RESULTS

The training outcomes of (MobilNet-v2, ResNet-18 and SqueezeNet) DCNN models are covered in this section. We used data sets [25] for this paper. There are two experiments in this study; In the first experiment, the suggested classifier, which has 8,903 instances for each class and a total of 17,806 datasets collected from the training dataset, extracted 14,245 skin photos for each class, 3,561 for the validation step, and 32 minimum batch sizes. The low-complexity CNN model's training phase involved the processing of these images. Ten epochs are used in the CNN model. Figure 10 shows the performance specifics of the training accuracy results from experiments (1) and (2).

Al-Furat Journal of Innovations in Electronics and Computer Engineering (FJIECE)
ISSN -2708-3985

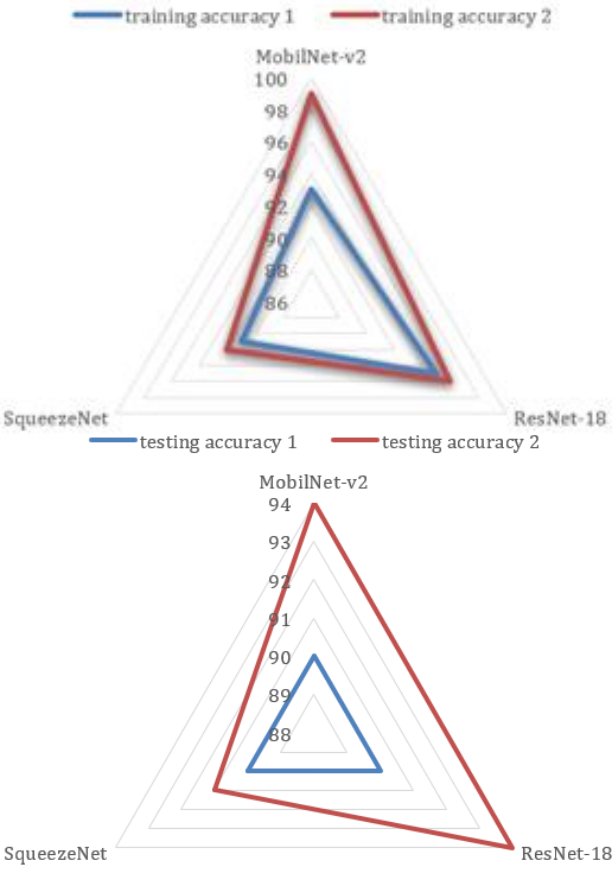

Figure 10: Comparison Results of Training and Testing Accuracy Between Experiment (1) With Experiment (2).

For Experiment-1 and Experiment-2 in (MobilNet-v2, ResNet-18 and SqueezeNet) DCNNs models respectively, The accuracy and loss are observed as seen in Figures below.

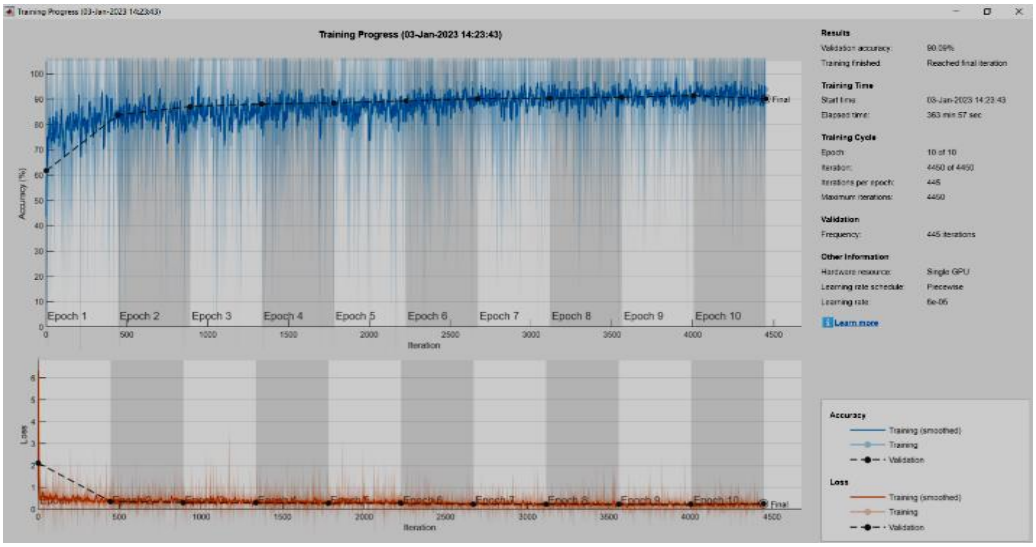

Figure 11: Accuracy and loss of Training for the Original Dataset in MobilNet-v2 (Experiment 1).

Al-Furat Journal of Innovations in Electronics and Computer Engineering (FJIECE)
ISSN -2708-3985

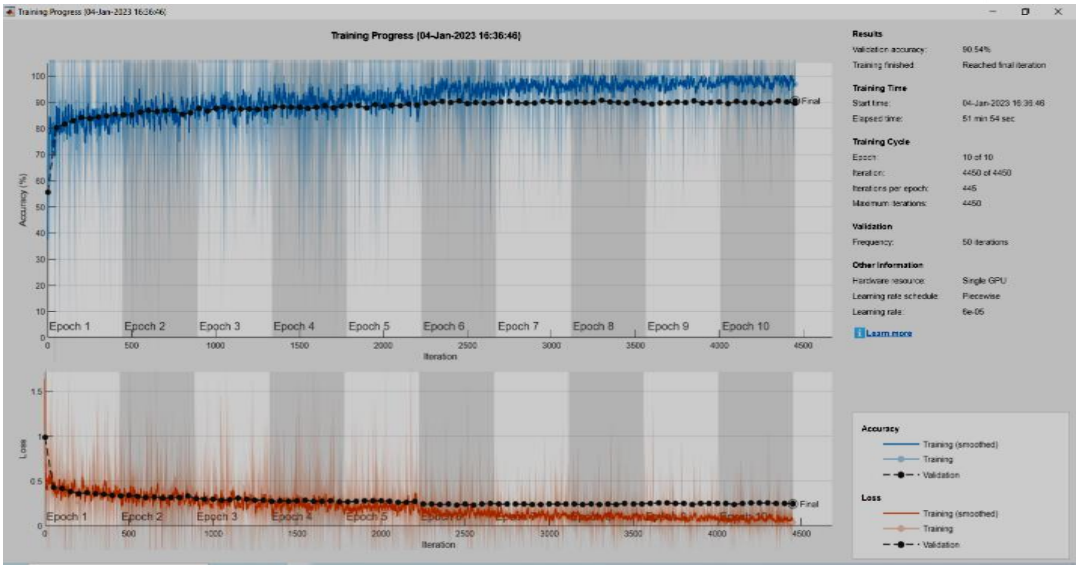

Figure 12: Results of Accuracy and Loss in Training for the Original Dataset in ResNet-18 (Experiment 1).

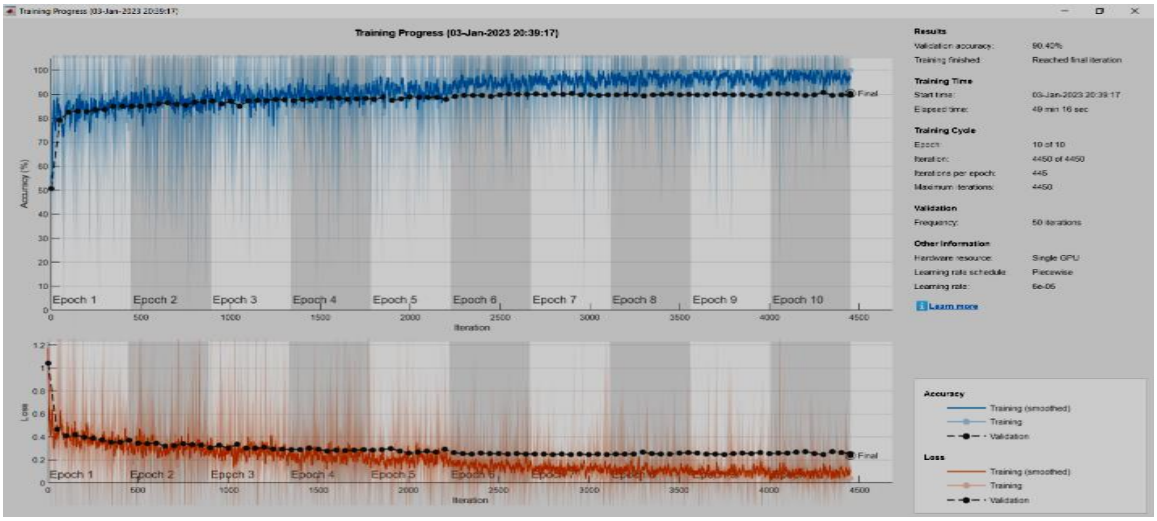

Figure 13: Results of Accuracy and Loss in Training for the Original Dataset in SqueezeNet (Experiment 1).

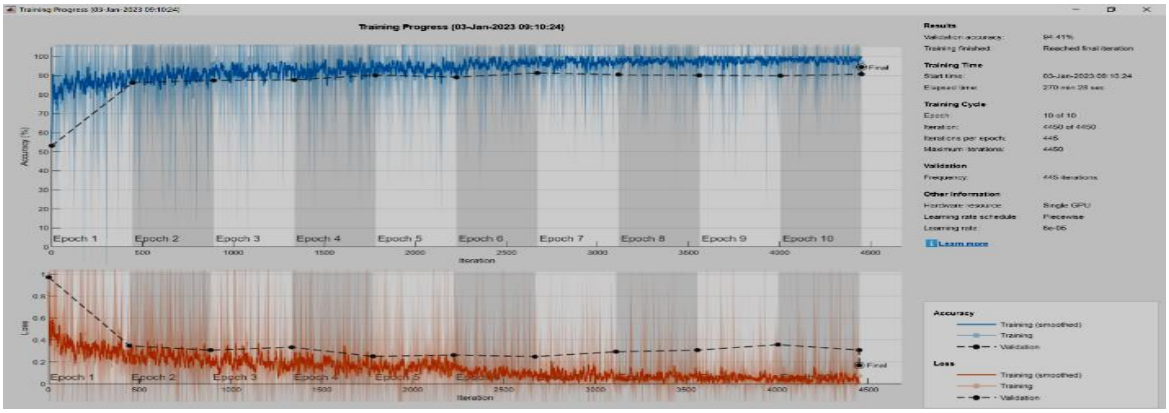

Figure 14: Results of Accuracy and Loss in Training for the Original Dataset MobilNet-v2 (Experiment 2).

Al-Furat Journal of Innovations in Electronics and Computer Engineering (FJIECE)
ISSN -2708-3985

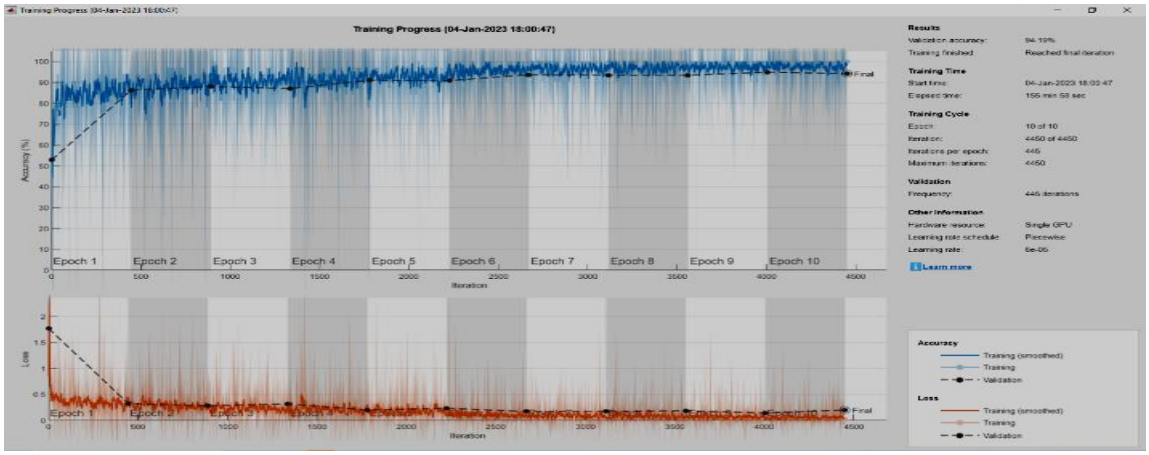

Figure 15: Results of Accuracy and Loss of the New Dataset's Training in ResNet-18 (Experiment 2).

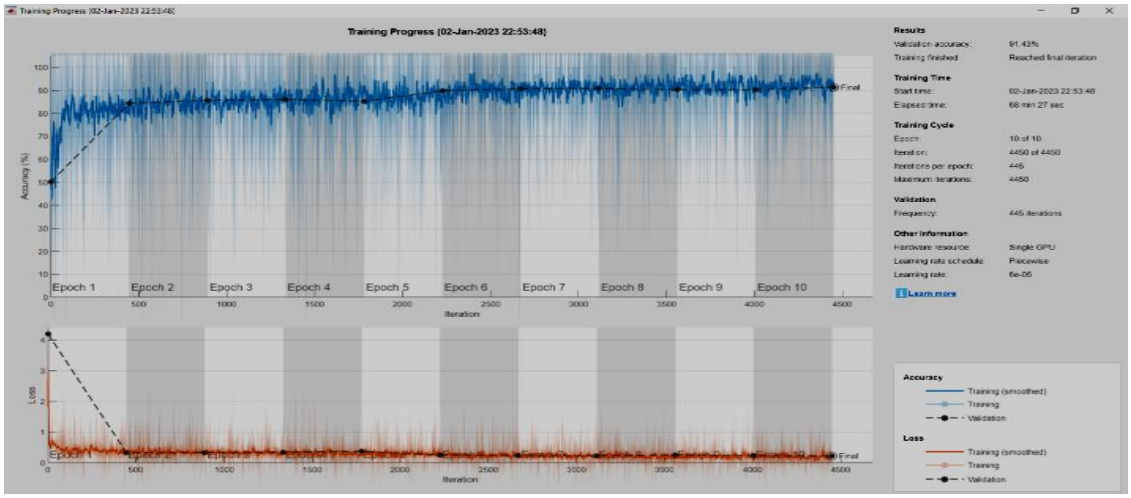

Figure 16: Results Accuracy and Loss of the New Dataset's Training in SqueezeNet (Experiment 2).

A confusion matrix for the training and testing dataset illustrates how well the model predicts the class used in supervised learning. The proposed model predicts the correct classes for the two classes in the validation test. Each column of the matrix represents the number of predictions for each class, whereas each row represents the actual class instances. The confusion matrix keeps track of the results, for experiment-1 and experiment-2 in (MobilNet-v2, ResNet-18 and SqueezeNet) DCNNs models respectively.

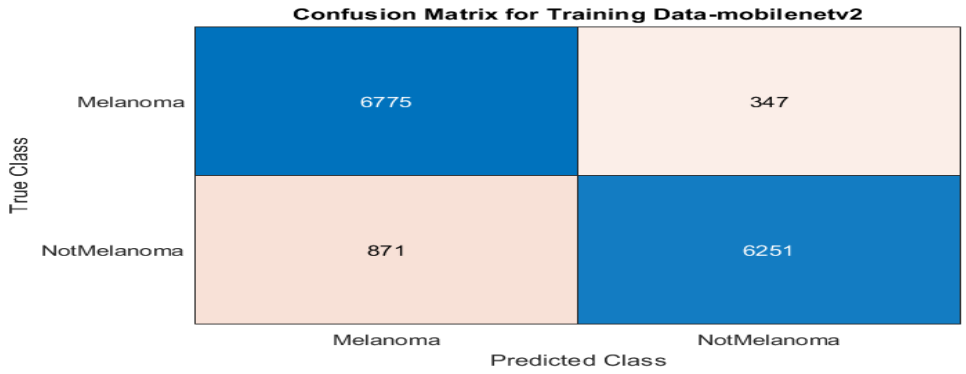

Al-Furat Journal of Innovations in Electronics and Computer Engineering (FJIECE)
ISSN -2708-3985

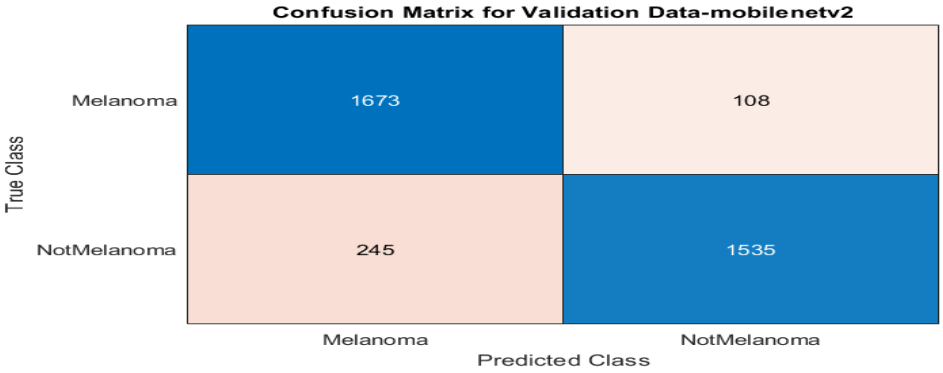

Figure 17: Results of Confusion Matrix in MobilNet-v2 Experiment 1

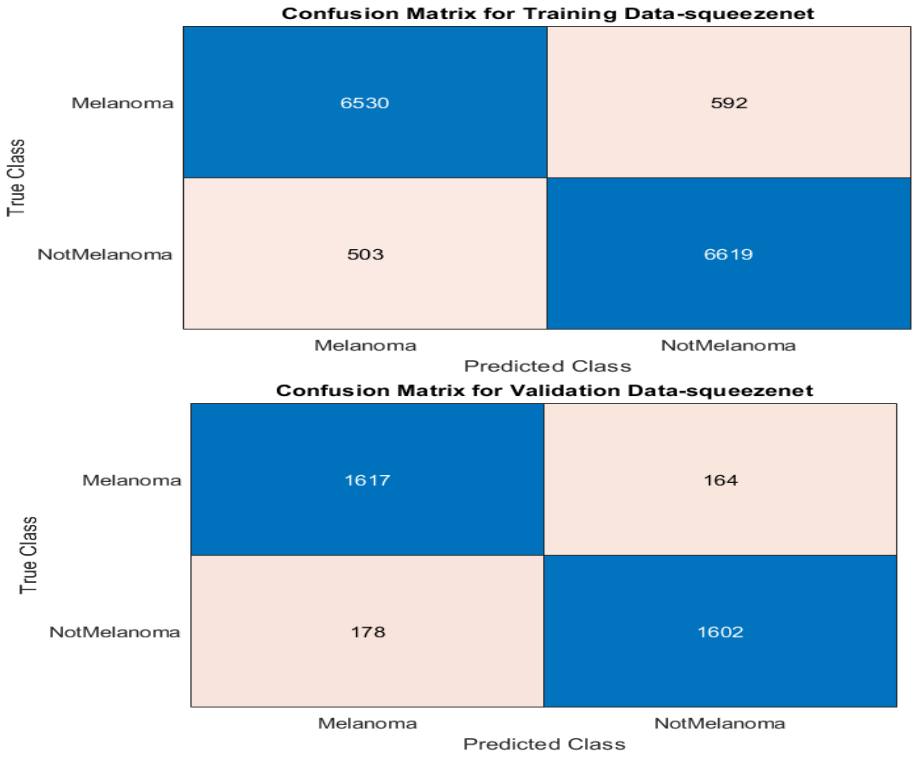

Figure 18: Results of Confusion Matrix in SqueezeNet Experiment 1

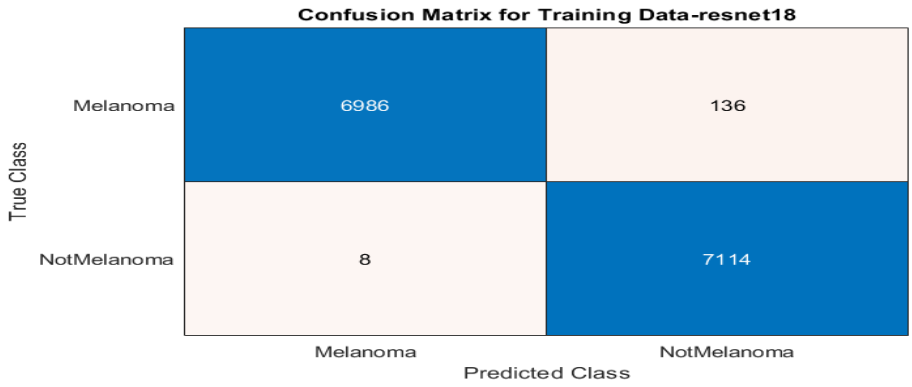

Al-Furat Journal of Innovations in Electronics and Computer Engineering (FJIECE)
ISSN -2708-3985

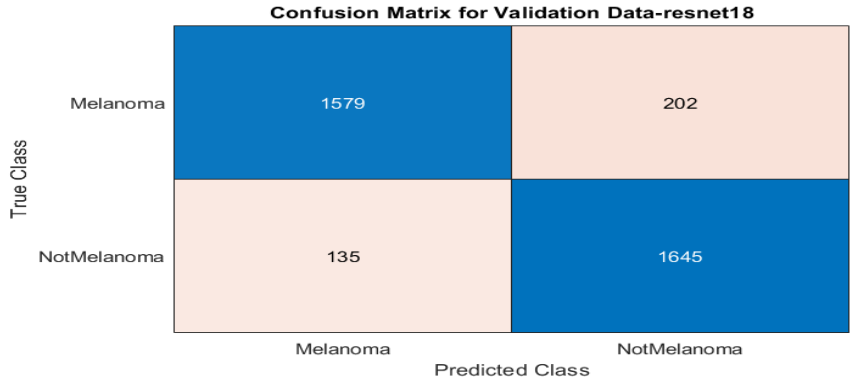

Figure 19: Results of Confusion Matrix in ResNet-18 Experiment 1

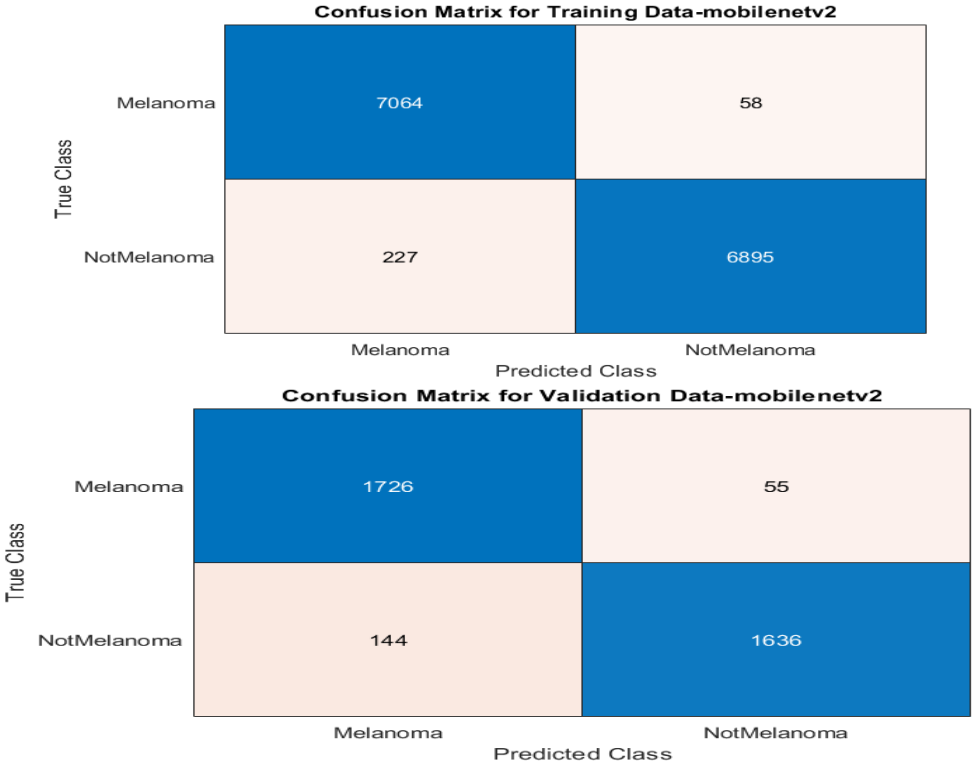

Figure 20: Results of Confusion Matrix in MobilNet-v2 Experiment 2

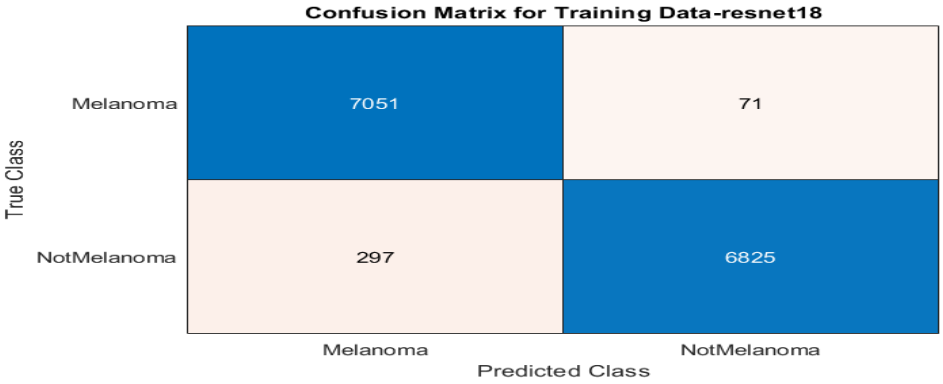

Al-Furat Journal of Innovations in Electronics and Computer Engineering (FJIECE)
ISSN -2708-3985

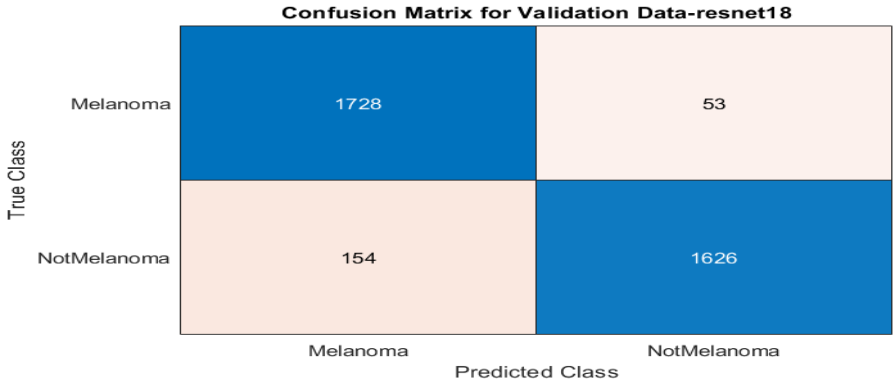

Figure 21: Results of Confusion Matrix in ResNet-18 Experiment 2

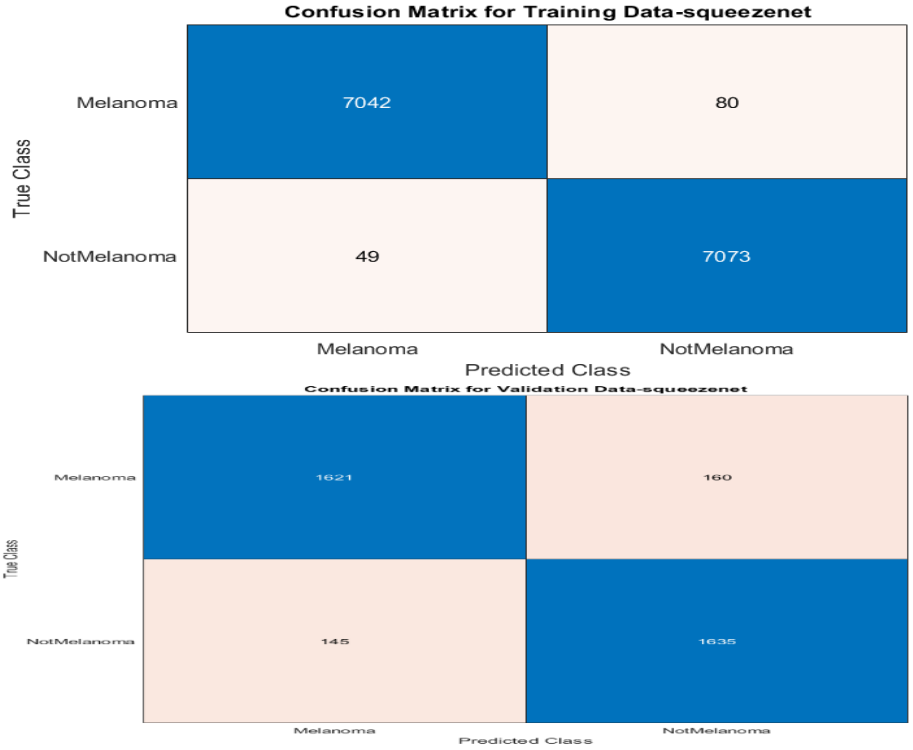

Figure 22: Results of Confusion Matrix in SqueezeNet Experiment 2

included in Table 2 below [32-33]. All computations (Accuracy, Specificity, Sensitivity/Recall, Precision, and F1-Score) are shown in Tab. 3.

Table 2 Illustrates the measurement of performance The metrics used to evaluate Accuracy, Specificity, Sensitivity/Recall, Precision, and F1-Score are TP, TN, FP, and FN.

True Positive TP	False Positive FP	$Precision = \frac{TP}{TP + FP}$

Al-Furat Journal of Innovations in Electronics and Computer Engineering (FJIECE)
ISSN -2708-3985

False Negative FN	True Negative TN	$Negative\ Predictve\ Value(NPV) = \frac{TN}{TN+FN}$
$Sensitivity\ Recall = \frac{TP}{TP+FP}$	$Specificity = \frac{TN}{TN+FP}$	$Accuracy = \frac{TP+TN}{TP+FP+TN+FN}$ $F1-Score = \frac{Precision\ +Recall}{Precision\ +Recall}$

To be more specific details of each class are in Tables 3, 4 & 5 for Experiment 1 and 6, 7 & 8 for Experiment 2.

Table 3: Results of Evaluation Training (MobilNet-v2) of Experiment 1

Category	Accuracy	Sensitivity	Specificity	Precision	F_measure
Melanoma	91	95	88	89	92
Nonmelanoma	91	88	95	95	91

Table 4: Results of Evaluation Training (ResNet-18) of Experiment 1

Category	Accuracy	Sensitivity	Specificity	Precision	F_measure
Melanoma	92	92	93	93	92
Nonmelanoma	92	93	92	92	92

Table 5: Results of Evaluation Training (SqueezeNet) of Experiment 1

Category	Accuracy	Sensitivity	Specificity	Precision	F_measure
Melanoma	99	98	100	100	99
Nonmelanoma	99	100	98	98	99

Table 6: Results of Evaluation Training (MobilNet-v2) of Experiment 2

Category	Accuracy	Sensitivity	Specificity	Precision	F_measure
Melanoma	98	99	97	97	98
Nonmelanoma	98	97	99	99	98

Table 7: Results of Evaluation Training (ResNet-18) of Experiment 2

Category	Accuracy	Sensitivity	Specificity	Precision	F_measure
Melanoma	97	99	96	96	97
Nonmelanoma	97	96	99	99	97

Table 8: Results of Evaluation Training (SqueezeNet) of Experiment 2

Category	Accuracy	Sensitivity	Specificity	Precision	F_measure
Melanoma	99	99	99	99	99
Nonmelanoma	99	99	99	99	99

5.Conclusions

Using three onclusions types of LWCNNs models (MobilNet-v2, ResNet-18 and SqueezeNet), we created a deep-learning method for classifying melanoma and non-melanoma skin lesions. This method makes use of picture enhancement as a preprocessing step to increase classification accuracy. Without any dataset augmentation, the results supported the comparison of the two scenarios. In the first, the obtained value of training accuracy is (93, 95 and 91) % and the testing accuracy are (90.09, 90.54 and 90.4) %, using original datasets only. In the second experiment, the obtained value of training accuracy is (99.7, 96.3 and 92) % and the testing accuracy are (94.41, 94.14 and 91.43) %, using a new dataset obtained from enhancing the features of skin scan images. From the experimental results, this work concludes that dataset preprocessing contributed to enhancing the classification output. Future research ideas include incorporating more datasets that have been endorsed by the World Health Organization as well as developing more effective techniques. Additionally, to speed up the execution of data analysis and assist medical professionals in the early detection of melanoma, an integrated system might be developed.

6.Conflicts of interest

"The authors affirm that they have no financial or other conflicts of interest to disclose about the current work".

REFERENCES

[1] N. Rezaoana, M. S. Hossain and K. Andersson, 2020 "Detection and classification of skin cancer by using a parallel cnn model," in Proc. 2020 IEEE International Women Engineering Conference on Electrical Computer Engineering (WIECON-ECE). pp. 380–386,.

[2] S. Nasiri, J. Helsper, M. Jung and M. Fathi, 2020 "DePicT melanoma deep-class: a deep convolutional neural networks approach to classify skin lesion images," in proc. 6th International Work-Conference on Bioinformatics and Biomedical Engineering Granada, vol. 21, no. 2, pp. 1–13,.

[3] A. A. Ali and H. Al-Marzouqi, 2017 "Melanoma detection using regular convolutional neural networks," in Proc. (ICECTA) ICECTA 2017, pp. 1–5,.

[4] M. C. Dalmau, S. Noé, M. O. Viñas, I. Meić and C. Manzo, 2021 "Convolutional neural network for skin lesion classification: understanding the fundamentals through hands-on learning," Frontiers in Medicine, vol. 8, pp. 1–8,.
[5] T. J. Brinker et al., "A convolutional neural network trained with dermoscopic images performed on par with 145 dermatologists in a clinical melanoma image classification task," European Journal of Cancer, vol. 111, pp. 148–154.
[6] C. H. Yang, J. H. Ren, H. C. Huang, L. Y. Chuang and P. Y. Chang, 2021 "Deep hybrid convolutional neural network for segmentation of melanoma skin lesion," Computational Intelligence and Neuroscience, vol. 2021, pp. 1-15,.
[7] Y. Ge, B. Li, Y. Zhao, E. Guan and W. Yan, 2018 "Melanoma segmentation and classification in clinical images using deep learning," in Proc. ACM, pp. 252–256,.
[8] A. Esteva et al., 2017 "Dermatologist-level classification of skin cancer with deep neural networks," Nature, vol. 542, no. 7639, pp. 115–118,.
[9] A. Sagar and D. Jacob, 2020 "Convolutional neural networks for classifying melanoma images," bioRxiv,.
[10] B. Nandini and R. Puviarasi, 2021 "Detection of skin cancer using inception v3 and inception v4 convolutional neural network (CNN) for accuracy improvement," Revistageintec Gestão Inovação e Tecnologias, vol. 11, no. 4, pp. 1138–1148,.
[11] R. Nersisson, T. J. Iyer, A. N. Joseph Raj and V. Rajangam, 2021 "A Dermoscopic skin lesion classification technique using YOLO-CNN and traditional feature model," Arabian Journal for Science and Engineering, vol. 46, no. 10, pp. 9797–9808,.
[12] K. M. Hosny, M. A. Kassem and M. M. Foaud, 2019 "Classification of skin lesions using transfer learning and augmentation with Alex-net," PLoS One, vol. 14, no. 5, pp. 1–17,.
[13] D. N. Anggraini Ningrum et al., 2021 "Deep learning classifier with patient's metadata of dermoscopic images in malignant melanoma detection," Journal of Multidisciplinary Healthcare, vol. 14, pp. 877–885,.
[14] I. Pölönen, S. Rahkonen, L. Annala and N. Neittaanmäki, 2019 "Convolutional neural networks in skin cancer detection using spatial and spectral domain," in Proc. SPIE BiOS, San Francisco, California, United States.
[15] H. A. Haenssle et al., 2018 "Man against Machine: Diagnostic performance of a deep learning convolutional neural network for dermoscopic melanoma recognition in comparison to 58 dermatologists," Annals of Oncology, vol. 29, no. 8, pp. 1836–1842,.
[16] A. Saad,"Melanoma and Non-Melanoma Classification Based on clustering channels RGB of skin scan". figshare. Dataset. https://figshare.com/articles/dataset/newdata_rar/19213812.
[17] A. G. Howard, M. Zhu, B. Chen et al., "Mobilenets: efficient convolutional neural networks for mobile vision applications," 2017, https://arxiv.org/abs/1704.04861.
[18] A. Saad, 2022 "Classification of COVID-19, normal and pneumonia based on enhancement X-ray image and squeeze Net model," CMC, vol.72, no.1,.
[19] Saad, A., Ahmed, J., Elaraby, A. (2022). Classification of bird sound using high-and low-complexity convolutional neural networks. Traitement du Signal, Vol. 39, No. 1, pp. 187-193. https://doi.org/10.18280/ts.390119.
[20] H. Z. Ali, S. Kabir and G. Ullah, 2021 "Indoor scene recognition using, ResNet-18," International Journal of Research Publications, vol. 69, no. 1, p. 7,.
[21] D. Zhu et al., 2020 "Geosot grid remote sensing intelligent interpretation model based on fine-tuning ResNet-18: a case study of construction land," in Proc. IGARSS 2020-2020 IEEE International Geoscience and Remote Sensing Symposium, pp. 2535–2538, Waikoloa, HI, USA,.

[22] D. Sarwinda, R. Paradise, A. Bustamam, and P. Anggia, 2021 “Deep learning in image classification using residual network (ResNet) variants for detection of colorectal cancer,” Procedia Computer Science, vol. 179, pp. 423–431,.
[23] F. Zeng, W. Hu, G. He and C. Yue, “Imbalanced Thangka image classification research based on the ResNet network,” Journal of Physics: Conference Series, vol. 1748, no. 4, pp. 042–054, 2021.
[24] K. He, X. Zhang, S. Ren, and J. Sun, 2015 “Deep residual learning for image recognition,” computer vision foundation,.
[25] N. Schaetti, “Character-based convolutional neural network and resnet18 for twitter author profiling notebook for pan at clef 2018.” PH.D. Theses, University of Gneva, Geneva, Switzerland, 2018.
[26] J. Zhao, Q. Zhu, Z. Du, T.Feng and Y. Zhang, 2012 "Mathematical morphology-based generalization of complex 3D building models incorporating semantic relationships," ISPRS Journal of Photogrammetry and Remote Sensing, vol. 68, pp. 95-111,.
[27] S. K. Mitra and H. Li, “A new class of nonlinear filters for image enshancement,” in Proc. IEEE Int. Conf. Acoustics, Speech, Signal Proscessing, Toronto, Ont., Canada, May 14–17, 1991, pp. 2525–2528.
[28] G. Ramponi, N. Strobel, S. K. Mitra and T. Yu, 1996 “Nonlinear unsharp masking methods for image contrast enhancement,” Journal of Electronic Imaging, vol. 5, no. 3, pp. 353–366,.
[29] J. Xiong, D. Yu, Q. Wang, L. Shu and J. Cen, “Application of histogram equalization for image enhancement in corrosion areas,” Shock and Vibration, vol. 2021, pp. 1-13, 2021.
[30] Xu, J., Gu, L., & Peters, T.M. (2005). A Novel Multistage,3D Medical Image Segmentation: Methodology and Validation. In proceeding of 2005 International Conference on Computational Intelligence and Security, Xi’an China.
[31] Jones & Soille, 1996; The MathWorks, 2004) The MathWorks, (2004). Image Processing Toolbox, For Use With MATLAB, Version 5. The MathWorks, Inc.
[32] A. Magotra and J. Kim, "Transfer Learning for Image Classification Using Hebbian Plasticity Principles", in Proc. CSAI 2019: 3rd International Conference on Computer Science and Artificial Intelligence, pp. 233–238, 2019.
[33] K. Weiss, T. M. Khoshgoftaar and D. D. Wang, " A survey of transfer learning," Journal of Big Data, vol. 3, no. 1, 2016.